

# Journal of Biomedical Optics

[SPIEDigitalLibrary.org/jbo](http://SPIEDigitalLibrary.org/jbo)

## **Optical clearing at cellular level**

Matti Kinnunen  
Alexander V. Bykov  
Juho Tuorila  
Tomi Haapalainen  
Artashes V. Karmenyan  
Valery V. Tuchin



**SPIE**

# Optical clearing at cellular level

Matti Kinnunen,<sup>a,\*</sup> Alexander V. Bykov,<sup>a</sup> Juho Tuorila,<sup>a</sup> Tomi Haapalainen,<sup>a</sup> Artashes V. Karmenyan,<sup>b</sup> and Valery V. Tuchin<sup>a,c,d</sup>

<sup>a</sup>University of Oulu, Optoelectronics and Measurement Techniques Laboratory, P.O. Box 4500, Oulu 90014, Finland

<sup>b</sup>National Yang-Ming University, Biophotonics and Molecular Imaging Research Center, Taipei 11221, Taiwan

<sup>c</sup>Saratov State University, Research-Educational Institute of Optics and Biophotonics, Saratov 410012, Russia

<sup>d</sup>Institute of Precise Mechanics and Control RAS, Laboratory of Laser Diagnostics of Technical and Living Systems, Saratov 410028, Russia

**Abstract.** Strong light scattering in tissues and blood reduces the usability of many optical techniques. By reducing scattering, optical clearing enables deeper light penetration and improves resolution in several optical imaging applications. We demonstrate the usage of optical tweezers and elastic light scattering to study optical clearing [one of the major mechanisms—matching of refractive indices (RIs)] at the single particle and cell level. We used polystyrene spheres and human red blood cells (RBCs) as samples and glycerol or glucose water solutions as clearing agents. Optical tweezers kept single microspheres and RBCs in place during the measurement of light scattering patterns. The results show that optical clearing reduces the scattering cross section and increases  $g$ . Glucose also decreased light scattering from a RBC. Optical clearing affected the anisotropy factor  $g$  of 23.25- $\mu\text{m}$  polystyrene spheres, increasing it by 0.5% for an RI change of 2.2% (20% glycerol) and 0.3% for an RI change of 1.1% (13% glucose). © 2014 Society of Photo-Optical Instrumentation Engineers (SPIE) [DOI: 10.1117/1.JBO.19.7.071409]

Keywords: optical clearing; single particle; elastic light scattering; red blood cell; optical tweezers.

Paper 130831SSPR received Nov. 20, 2013; revised manuscript received Jan. 21, 2014; accepted for publication Feb. 12, 2014; published online Mar. 10, 2014.

## 1 Introduction

During the last 10 years, optical methods have been developed for tissue imaging and therapy. However, their resolution and imaging depth are limited by strong light scattering in tissue. Light propagation in tissues is determined by macroscopic optical parameters, such as optical absorption  $\mu_a$ , optical scattering  $\mu_s$ , scattering anisotropy factor  $g$ , and refractive index (RI)  $n$ . Manipulation of the RI of tissue has been shown to enhance the usability of optical techniques both in the microscopic and macroscopic scales. Optical immersion clearing is a promising technique that enables measuring the RI of cells and cellular components. As phase-contrast microscopy is a nonlabelling imaging method applicable to cell analysis, exact information of the RIs of cellular components is essential for analysis.<sup>1–3</sup> Recent studies also show that cell-level contrast can be enhanced by altering the cytoplasmic RI.<sup>4</sup>

Optical penetration depth in tissue can be increased, and multiple scattering can be reduced by the use of optical clearing agents (OCAs). In practice, this often means matching the RIs of scattering particles and the surrounding medium.<sup>5–7</sup> Optical clearing in tissue comprises different processes, such as water outflow/replacement as well as chemical alterations in intracellular and extracellular substance concentrations. Reversible tissue dehydration due to the osmotic properties of OCAs results in more densely packed tissue structures and reduced thickness.<sup>5–7</sup> In addition to reduced scattering, the absorption spectrum of the studied sample may change. Changes in the shape of the cell (induced by osmolarity, for instance) will affect its anisotropy ( $g$ ), i.e., directivity of light propagation in a scattering event.<sup>6</sup>

Blood exhibits very high absorption in the visible spectral range, and blood components (hemoglobin in particular) reduce light penetration considerably. In addition, red blood cells (RBCs) scatter light significantly in the wavelength range of 450 to 1050 nm.<sup>8,9</sup> Hence, optical clearing of blood avails itself to interesting specific applications, such as imaging or controlling the functioning of a tissue within the area of agent action.<sup>6</sup> The main mechanisms of optical clearing are RI matching and RBC aggregation.<sup>9–13</sup> In addition, RBCs easily change their shape according to the osmotic environment of the medium (e.g., plasma). Also, theoretical modelling supports blood optical clearing by hemoglobin and glucose.<sup>14,15</sup>

Light scattering patterns enable quantifying various parameters of RBCs, including mean cell volume and mean cell hemoglobin concentration (MCHC).<sup>16</sup> This information can be utilized by flow cytometry devices and blood cell counters. Various parameters have been shown to affect the optical properties of blood. When studying osmotic effects and corresponding changes in optical properties, Friebe et al.<sup>17</sup> found that changes in cell volume affect hemoglobin concentration and, consequently, the RI of the cell. This can be seen as increased light scattering. In the wavelength range of 600 to 1100 nm, the value of  $g$  is linearly dependent on osmolarity.

Microscopy and its variations can be used to explore biological structures and light-matter interactions.<sup>18–24</sup> This enables studying light scattering properties and optical clearing at the single cell level. Popescu et al.<sup>25</sup> have demonstrated RI matching induced by hemoglobin during hemolysis. Also, the study of other OCAs at the single cell level has attracted considerable interest. Ding et al.,<sup>18</sup> Park et al.,<sup>19</sup> and Kim et al.<sup>20</sup> measured light scattering from RBCs, and quantified the difference between malaria-infected and normal cells, as well as showed

\*Address all correspondence to: Matti Kinnunen, E-mail: [matti.kinnunen@ee.oulu.fi](mailto:matti.kinnunen@ee.oulu.fi)

the potential for differentiation of sickle cells from normal RBCs. Optical tweezers can be used to keep cells in place during scattering measurements.<sup>26–30</sup> Kinnunen et al. studied the effect of osmotic changes on light scattering,<sup>26</sup> as well as dependent scattering of double RBCs.<sup>31</sup> Here, we propose to use optical tweezers accompanied with a goniometric measurement system to measure optical clearing-induced changes on the micrometer scale. The main focus of this study is to measure the effect of selected OCAs, namely glycerol and glucose, on the scattering phase function at the single particle and RBC level. This will increase our understanding of basic light-tissue interaction at the cellular level under application of clearing agents, which may lead to new applications, for example, in the area of intravenous blood vessel imaging<sup>14,32,33</sup> or RBC membrane permeability and rigidity.<sup>25</sup>

## 2 Theoretical Considerations

For a single particle, the scattering cross section and mean cosine of the scattering angle  $\theta$  (scattering anisotropy factor  $g = \langle \cos \theta \rangle$ ) can be calculated using the Mie theory.<sup>34</sup> In a form suitable for experimental evaluations, the average scattering cross section per particle can be presented as<sup>34</sup>

$$\sigma_{\text{sca}} = (\lambda^2/2\pi)(1/I_0) \int_0^\pi I(\theta) \sin \theta d\theta, \quad (1)$$

where  $I_0$  is the intensity of the incident light,  $I(\theta)$  is the angular distribution of the light scattered by the particle and  $\theta$  is the scattering angle. For a dielectric sphere (Mie theory) with parameters close to a RBC irradiated by visible or NIR light ( $g > 0.9$ ,  $5 < \pi d/\lambda < 50$ ,  $1 < m < 1.1$ ), the scattering cross-section is described as<sup>35</sup>

$$\sigma_{\text{sca}} \sim [d^2(d/\lambda)^{0.37}(m-1)^{2.09}]/(1-g), \quad (2)$$

where  $d$  is the particle diameter,  $\lambda$  is the light wavelength,  $m \equiv n_s/n_0$  is the relative RI of the particle that determines its scattering ability,  $n_s$  is the RI of the scatterer,  $n_0$  is the RI of the surrounding medium, and  $g$  is the scattering anisotropy factor, defined as a mean cosine of the scattering angle  $\theta$ ,

$$g \equiv \langle \cos \theta \rangle = \int_0^\pi p(\theta) \cos \theta \cdot 2\pi \sin \theta d\theta, \quad (3)$$

where  $p(\theta)$  is the phase function that describes the scattering properties of the particle and is, in fact, the probability density function for scattering in some direction of a photon travelling in the other direction; in other words, it characterizes an elementary scattering act. If scattering is symmetric relative to the direction of the incident wave, then the phase function depends only on the scattering angle  $\theta$  (the angle between these two directions).

From Eq. (2), it follows that matching the RIs of a scatterer (particle or cell)  $n_s$  and its surrounding medium  $n_0$  may lead to a considerable reduction of the scattering cross section. As a consequence of the greater directness of scattering that results from RI matching, the mean cosine ( $g$ -factor) tends to unity.<sup>36</sup> If RI matching is achieved by the use of hyperosmotic OCAs, cell shrinkage can be expected, which, due to decreased cell diameter, may lead to a further reduction of the scattering cross-section [see Eq. (2)].

Using Eq. (2), the scattering cross-section alteration at RI matching conditions can be estimated as

$$(\sigma_{\text{sca}})_m/(\sigma_{\text{sca}})_{\text{unm}} = [(m_m - 1)/(m_{\text{unm}} - 1)]^{2.09} \times [(1 - g_{\text{unm}})/(1 - g_m)], \quad (4)$$

where the subscript “m” refers to matched and the subscript “unm” to unmatched conditions.

## 3 Method and Materials

### 3.1 Measurement Setup

For trapping, we used a laser with an output power of 350 mW at the wavelength of 1064 nm (ILM-L3IF-300 diode module, LeadLight Technology, Taiwan). Beam propagation in the system has been described in detail in recent publications.<sup>30,37</sup> We used a water immersion objective (Olympus LUMPLFL100XW/1.00, Japan) with a magnification of 100× and a working distance of 1.5 mm. The numerical aperture of the objective was 1.0, thus ensuring efficient trapping. A long working distance was necessary to decrease He-Ne laser light reflections from the tip of the objective, thereby reducing its effect on our measurements. Samples are illuminated with a halogen lamp via an optical fiber and imaged with a high-speed video camera (Centurio100, Citius Imaging, Mathildedal, Finland). The sample chamber was placed on an adjustable sample stage, mounted on a motorized  $xy$  stage (Thorlabs MAX201, Göteborg, Sweden).

The setup for measuring light scattering on the illumination side consisted of a linearly polarized He-Ne laser (MellesGriot, Carlsbad, California), a focusing lens (+200 mm) and a pinhole. On the detecting side, the setup consisted of three apertures, a lens on a steerable mount, an IR dichroic hot mirror (Thorlabs FM01), a photomultiplier tube (PMT) (Hamamatsu, Solna, Sweden, H9305-04), a preamplifier (Stanford Research Systems, Sunnyvale, California, SR445A), a photon counter (Stanford Research Systems, SR400), and a computer. The detector was moved around the sample with a motorized rotation stage (Standa 8MR190-2-28, with 8SMC1-USBhF-B1-1MC controller, Vilnius, Lithuania), using an angle step of 0.1 deg for polystyrene spheres and 0.5 deg for RBCs. LabView 8.5.1 software was used to control the movement of this rotation stage and for data acquisition. Rotation speed was 37 steps in a minute. For our experiments, samples were placed in a 15-mm-high cylindrical cuvette (shortened version of Hellma 540.115, Müllheim, Germany) with an inner diameter of 22.6 mm and an outer diameter of 25 mm. All measurements were repeated three times and averaged signals are plotted in the figures.

Particles and cells were added to the bottom of the cuvette and allowed to settle. Optical trapping power of 225 mW (laser before objective) was used to keep the cell or particle under study in place during the measurement and to lift it from the bottom of the cuvette. Only a single particle or cell was picked up at a time for measurement. The illuminating He-Ne laser had a power of about 5.8 mW. First, the scattering signal was measured several times from the trapped particle. Then, the trapping laser was closed and the background signal from the surroundings was measured. Figure 1 shows a schematic of laser light scattering from a trapped cell.

### 3.2 Modeling

Light scattering from single spheres was modelled with Mie-theory software (MiePlot software version 4.3 was downloaded from Ref. 38). By inserting the necessary parameters  $n_s$ ,  $n_0$ ,  $r$ ,

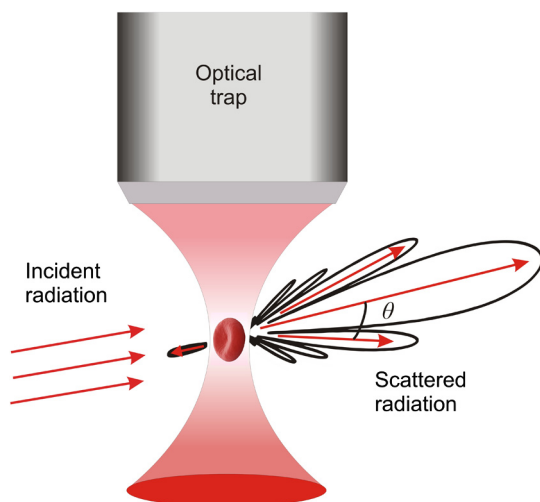


**Fig. 1** Schematic of the light scattering basics of the cell in trap.

and  $\lambda$ , scattering patterns were plotted and  $g$  values calculated. The values of RIs used in the calculations were 1.59 for a polystyrene sphere and 1.41 for a RBC.<sup>39</sup>

### 3.3 Materials

As a first stage model to studying RI matching, we used 23.25- $\mu\text{m}$  polystyrene spheres (Bangs Lab, Fishers, Indiana) suspended in distilled water. The RBC mass in a nutrition medium was obtained from the Finnish Red Cross and stored in a refrigerator at 4°C. The RBCs were centrifuged with phosphate buffered saline (PBS) three times, and a small RBC concentration was diluted for measurements with PBS. Fixed RBCs were prepared using commercially available 25% glytaraldehyde (GA) (Merck, Darmstadt, Germany). 1% GA was used with washed RBCs (with the PBS removed) for 30 to 40 min; then washed with water. This procedure was adapted from Refs. 40 and 41. For optical clearing experiments, distilled water and PBS (Sigma Aldrich, Steinheim, Germany, D8537) were filtered three times with a filter pore size of 1.0  $\mu\text{m}$  (Whatman, Buckinghamshire, United Kingdom) before mixing the liquids. The final mixture (glycerol or glucose) was filtered once.

The following clearing agents were used in the experiments at different concentrations: 99.5% glycerol (G7893, Sigma Aldrich) and glucose (Calbiochem, Germany). Table 1 shows concentrations of the prepared samples and measured RIs at two wavelengths [Refractometer Atago DR-M2 1550 (Atago,

**Table 1** Measured refractive indices (RI) of the sample at two wavelengths.

Sample	RI 633 nm	RI 1100 nm
5% Glucose	1.339	1.331
13% Glucose	1.347	1.338
20% Glycerol	1.361	1.352
Phosphate buffered saline (PBS)	1.333	1.325
Water	1.331	1.323

Japan)]. Of these, 633 nm was used in light scattering measurements, while 1100 nm is close to the trapping wavelength of 1064 nm.

## 4 Results and Discussion

One of the mechanisms of optical clearing involves matching the RIs of scattering particles and their surrounding environment.<sup>7</sup> Factors that affect the RI include concentration of the scatterers as well as the concentration of the solution (e.g., 20% glycerol).<sup>2,3</sup> Our experimental results show [Fig. 2(a)] that when increasing the RI of the surrounding medium by 2.2%, changes in the scattering phase function occur both in the intensity and position of scattering intensity maxima. This result has been verified by modelling [Fig. 2(b)]. The modeled signal shown in the figure represents the unpolarized case, because the measurement setup could not differentiate the effect of polarization on the measurements (data now shown). Hence, we obtained a good match between experimental results and modeling. Figure 3(a) shows corresponding measurements for 13%-glucose, where the RI increases only by 1.2%, whereas Fig. 3(b) shows corresponding modelling results. As seen, the effect on actual measured signals show similar tendency.

The anisotropy parameter  $g$  was calculated both for modelled and measured signals (see Tables 2 and 3). As the angular range used in the calculations affects the final value, the  $g$ -value is different for the whole curve (180 deg) than for a specific range (10 to 120 deg). This particular range was selected, because the measured signals were taken within it. In all cases, clearing served to increase the value of  $g$ . For 20% glycerol, the change was 0.5%, whereas that for 13% glucose was 0.3%. It can be seen that the  $g$ -values estimated from the measurements are somewhat smaller than those calculated from the full curve.

Optical clearing of cells is less straightforward. It is well known from the literature (both theoretical and experimental results) that the orientation and shape of the cell affects light scattering patterns. So, do the osmotic properties of the surrounding medium.<sup>30,42–45</sup> Hence, the effect of adding OCA to the sample medium can be multifaceted.

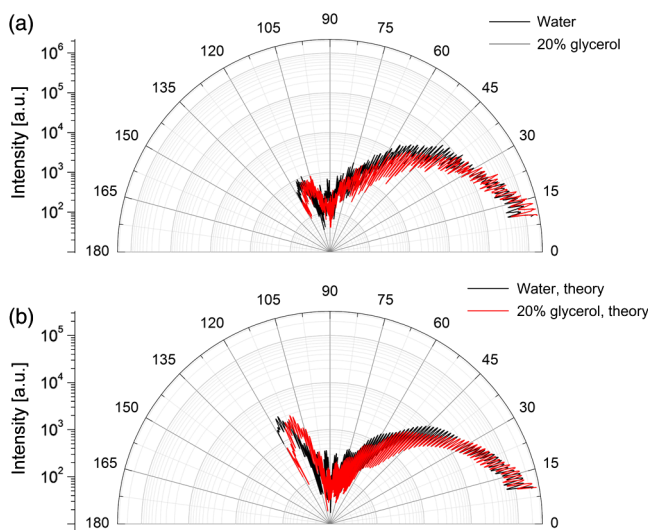


**Fig. 2** Light scattering phase functions from a single polystyrene sphere. (a) Measurement in water and water-glycerol mixture, (b) modeling in corresponding conditions. 20% glycerol-water mixture is used.

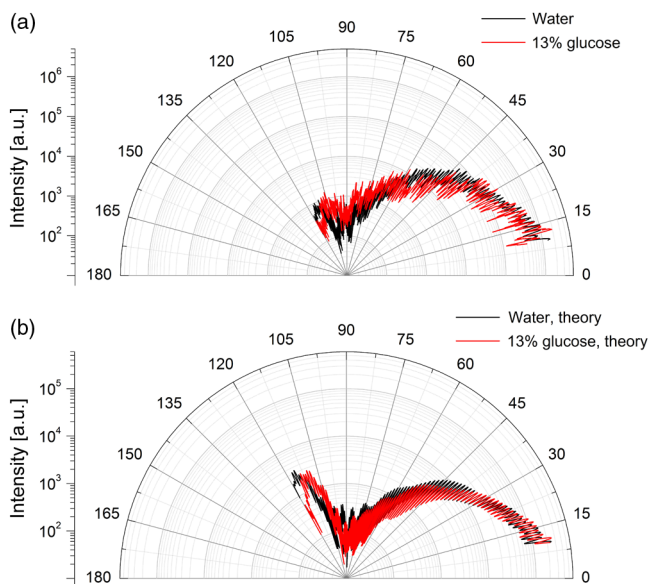


**Fig. 3** Light scattering phase functions from a single-polystyrene sphere. (a) Measurement in water and water-glucose mixture, (b) modeling in corresponding conditions. 13% glucose solution is used.

Fixed cells were prepared to limit the effect of changes in the shape of RBCs during optical trapping and scattering measurements, and a 5% glucose solution was used for clearing. Figure 4 shows camera images of a trapped cell during an experiment. As Fig. 5 indicates, some changes can be observed in scattering pattern shapes. The RI change, however, is too small for clearly observable changes in intensity level, but changes in the shape of scattering light intensity distribution are more obvious.

Figure 6 shows that the fixation process did not significantly affect the optical properties of RBCs, because scattering intensity remains at the same level before and after fixation. Changes in orientation are expected to be the reason for changes in intensity distribution.

We also modelled light scattering from a spherical RBC (unpolarized light). It is known that single RBCs can be modelled as oblate spheroids,<sup>39</sup> while a suspension of RBCs can be modelled as a system of randomly distributed spherical

particles, whose equivalent volume equals that of nonspherical models.<sup>46,47</sup> Each sphere had a RI of 1.41 and a diameter of 5.5  $\mu\text{m}$ . Figure 7 shows the scattering intensity distribution for unpolarized light in three different conditions: (1) RBC in PBS, (2) RBC in a glucose-PBS suspension, and (3) RBC in a glycerol-PBS suspension. 13% glucose concentration and 20% glycerol concentration was used in the calculations. The RI values for the background were taken from Table 1. We also calculated the anisotropy parameter  $g$  for a spherical RBC model (Table 2). The modelling in Fig. 8 shows a change in the RI of the medium that corresponds to the experimental situation in Fig. 5 (5% glucose).

The RI matching increases  $g$  and decreases the scattering cross section (Table 2). In addition,  $g$  is also strongly affected by particle size. Experimental results show that adding glucose to the base medium increases its RI (Table 1). At the same time, scattering from the background medium also increases. This makes it very challenging to measure small light scattering signals, when using glucose as a clearing agent. Figure 5 presents  $g$ -values calculated for the measured curves. Missing data points in the measured curves were padded with approximated values (Table 3), giving slightly different  $g$ -values for the cells. To replace missing data, basic spline approximation was used. Alternatively, we have compared calculated  $g$ -values to those obtained with zero padding. It was found that zero padding gives a 1.5% smaller value for the calculated anisotropy factor  $g$ .

Optical properties of blood depend on the used wavelength. When studying whole blood, absorption and scattering properties are handled as a probability of scattering and absorption events occurring. Roggan et al.<sup>8</sup> conducted a set of experiments and compared their results with Mie theory calculations. They found that scattering depends largely on cell volume and RI, while the shape of the RBC plays a minor role. Also, the RBC surface has a small effect. However, Friebel et al.<sup>17</sup> later discovered that the Mie theory does not explain all experimental results. Their results suggest that cell shape must also be considered in any practical model. Our measurements, presented in Ref. 30, also show that the shape and orientation of cells makes a significant contribution to light scattering patterns. For example, in optical coherence tomography the backward scattered signal contains important information.

**Table 2** Calculated values for optical clearing-induced changes in anisotropy and scattering cross sections. Measured RI values were used and they were taken from Table 1.

Sample	Diameter ( $\mu\text{m}$ )	Anisotropy (full curve model)	Change in anisotropy (%)	Scattering cross section alteration [Eq. (4)]
Polystyrene sphere, water	23.25	0.918	—	—
Polystyrene sphere, water + glucose 13%	23.25	0.931	1.40	1.02
Polystyrene sphere, water + glycerol 20%	23.25	0.934	1.75	0.92
RBC spherical model, PBS	5.5	0.990	—	—
RBC spherical model, PBS + glucose 5%	5.5	0.992	0.17	—
RBC spherical model, PBS + glucose 13%	5.5	0.994	0.31	0.94
RBC spherical model, PBS + glycerol 20%	5.5	0.995	0.49	0.75

**Table 3**  $g$ -Factor calculations from the measurements.

Sample	Diameter ( $\mu\text{m}$ )	Anisotropy (partical curve, model)	Anisotropy (from measurements, range 10 to 120 deg)
Polystyrene sphere, water	23.25	0.844	0.890
Polystyrene sphere, water + glucose 13%	23.25	0.860	0.892
Polystyrene sphere, water + glycerol 20%	23.25	0.862	0.915
Fixed RBC, PBS, measured (Fig. 5)	—	—	0.877 <sup>a</sup>
Fixed RBC, PBS + glucose 5%, measured (Fig. 5)	—	—	0.944 <sup>a</sup>
RBC in PBS (Fig. 6)	—	—	0.931 <sup>a</sup>

<sup>a</sup>Missing values in the measurements were filled with approximated values.

Optical clearing of blood aims to reduce scattering and enhance light penetration. Some differences have been found between *in vitro* and *in vivo* clearing. Key mechanisms here are RI matching and RBC aggregation. In addition, sedimentation

plays an important role in *in vitro* experiments.<sup>9</sup> On the other hand, flowing blood induces shear stress and decreases aggregation-induced clearing.<sup>13</sup> Some other processes in blood may also influence light scattering by RBCs. Friebel et al.<sup>17</sup> show that in the case of low absorption (diluted blood, wavelength range of 600 to 1100 nm), decreasing the volume of RBCs by 12% to 13% decreases the anisotropy factor by 0.01. They took into account the increasing RI of cells when the hemoglobin concentration within them increases. In our OCA experiment, we found the opposite effect; i.e., matching of RIs serves to decrease  $m$  and increase  $g$ , when the volume and RI of the scatterer remain unchanged.

Our experimental results show that, in the case of rigid polystyrene spheres, RI matching produces a clearing effect and there is a clear shift in the minima and maxima of the scattering pattern, when the relative RI  $m$  decreases. These results are supported by theoretical predictions. We also established that the  $g$ -factor increases with the application of OCAs. Controlled experiments using RBCs, however, proved more challenging. Theoretical model predicts that a decrease in the volume of a cell due to the osmotic effect will increase its RI, and that the increasing RI of the surrounding medium will be hardly detectable. Thus, the initial effect will be increased scattering.<sup>48</sup> Therefore, we used fixed RBCs to stabilize experimental conditions and minimize the effect of shape changes.

Theoretical and experimental papers show that optical clearing by hemoglobin is feasible at the single cell level.<sup>14,25</sup> In this article, we show how the use of glycerol and glucose affects light scattering distributions at the single particle and cell level.

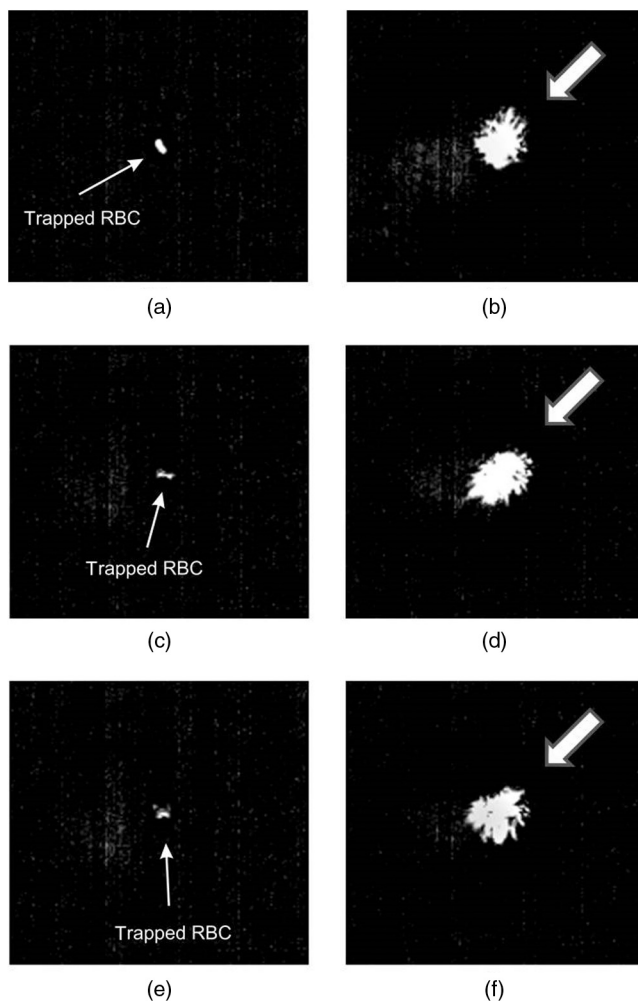


**Fig. 4** Microscope images of light scattering from trapped red blood cell (RBC). (a) fixed RBC + glucose, (b) fixed RBC + glucose He-Ne laser on, (c) fixed RBC, no glucose, (d) fixed RBC, no glucose, He-Ne laser on, (e) RBC in PBS, no fixation, (f) RBC in PBS, He-Ne laser on. The thick arrows show the direction of incident laser light.

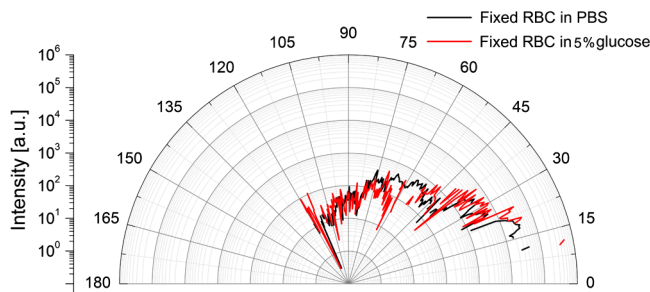


**Fig. 5** Light scattering patterns from the cells in Figs. 4(a) and 4(c). Light scattering intensities are shown in Figs. 4(b) and 4(d).

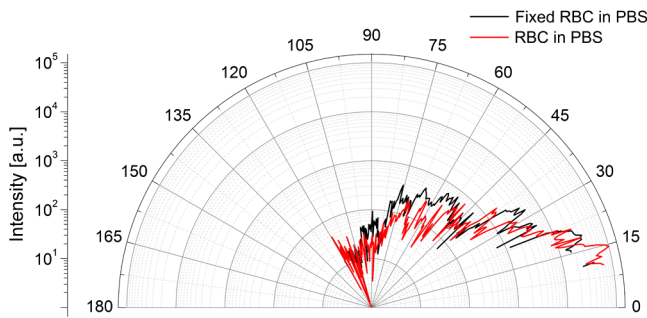


**Fig. 6** Light scattering patterns from RBC without fixation and from fixed RBC. Shape variation can be clearly seen from the light scattering intensity.

It must be pointed out that the surrounding medium, i.e., PBS with different concentrations of OCAs, differs from blood plasma. The RI of blood plasma and that of the studied samples resemble each other, but the proteins of plasma make the situation much more complicated and difficult to compare directly. From the measurement point of view, the background must be as clear as possible. Therefore, it is not possible to measure light scattering from RBCs in plasma suspensions with our current setup. Also other biomolecules, such as dextran or glucose, increase background scattering, which distorts the measurements.<sup>49</sup>

The specificity of this experiment results from combining optimal conditions for two phenomena, determined by the RI difference between a sample and its environment. To facilitate optical clearing, it is necessary (desirable) to increase the refractive index of the cell's environment in order to reduce light scattering by the cell. On the other hand, stable optical trapping requires a certain relationship between these refractive indices, and their values cannot be too close to each other.<sup>50</sup>

In these measurements, the function of optical tweezers is noninvasive, keeping a particle or cell in a fixed position for a significant length of time. Trapping efficiency is numerically characterized by a dimensionless value,  $Q$ . One important factor in this context is the influence of the effective index of refraction on the gradient force (ratio  $n_s/n_0$ ). A successful laser trap with a trapping efficiency of  $>90\%$  can be achieved over the range of  $n_s/n_0 = 1.1$  to  $1.6$  (Ref. 51). As mentioned earlier, there is wide variation in the efficiency of the trap in practically identical conditions, which also demonstrates how strongly dependent efficiency is on a right combination of all conditions.<sup>52</sup>

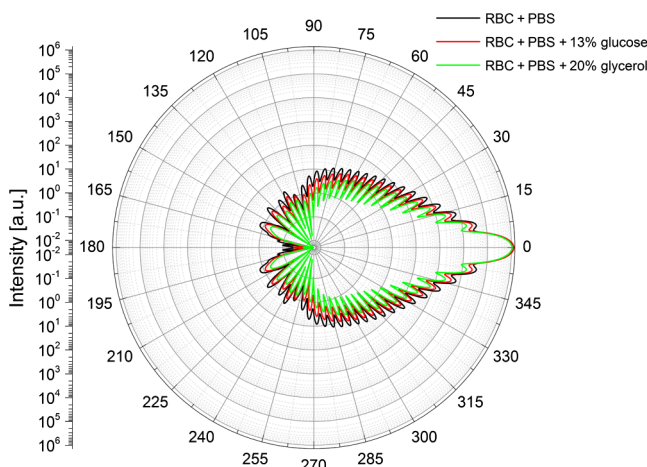


**Fig. 7** Light scattering from a spherical model RBC, unpolarized light.

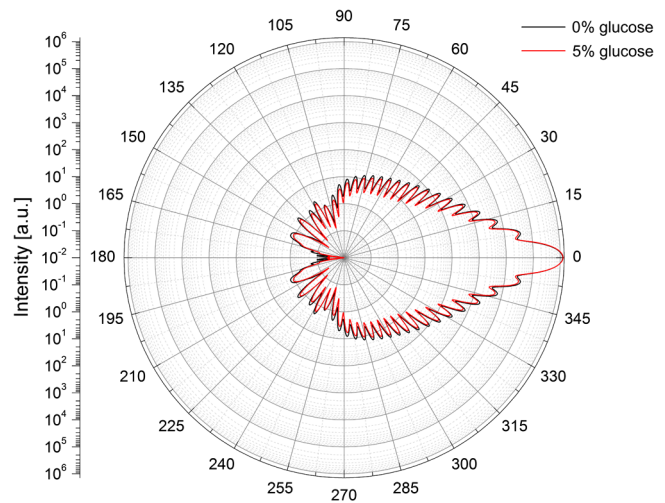


**Fig. 8** Light scattering from a spherical RBC, effect of 5% glucose.

On one hand, introducing additional components to a medium to match its RIs with that of the cell membrane may worsen trapping conditions (due to approximation of the RIs). On the other hand, this increases the medium's viscosity, making it harder for the object to escape from the trapping point.

An analysis of trapping efficiency was conducted for ray optics approximation (Mie approximation).<sup>50</sup> Numerical estimations show that when  $n_s/n_0$  is equal to 1.05 (difference of  $\sim 5\%$ ), trapping efficiency reaches about 60% of maximum possible efficacy. In practice, this corresponds to a RBC in a PBS,<sup>53</sup> which also shows a relatively stable trap and allows carrying out measurements.<sup>29,54</sup>

It is significant that these experiments do not require that the applied laser power is close to the trapping threshold values (as is the case, for example, in calibrations or force measurements). In experiments with biological cells, excessively high-laser power must be avoided to avoid cell damage. Additionally, it is well-known that trapping efficiency significantly depends on the distance between the object and the cuvette surface and decreases with increasing distance: this dependence is more manifest for particles of small size ( $\sim 1 \mu\text{m}$ ) than for larger ones.<sup>55,56</sup> In our experiments, we placed the particle far from the cuvette surface to eliminate unwanted background signals and reflections of the probing beam from cuvette walls.

Light scattering at the single cell level has been studied with optical tweezers. These studies have shown that intracellular components have an effect on light scattering patterns.<sup>28</sup> Optical clearing phenomena and its effects have been studied in other types of cells than RBCs. For example, Ref. 57 presents experimentally determined scattering intensity ratios from cells (rat fibroblast cell clone MR1;  $\sim 10^5$  cells/mL) immersed in media with low- and high-refraction indices. Having a refractive index of  $n = 1.332$ , PBS was used as the low-RI medium. Bovine serum albumin in PBS, with a RI of  $n = 1.345$ , and ovalbumin in PBS, with  $n = 1.343$ , served as media of higher index of refraction. At small angles ( $<20$  deg), scattered light intensity was significantly greater, when the cells were immersed in PBS with a low RI than in a protein solution with a high index. Thus, it may be concluded that there is significant scattering at small angles from cell structures that are in contact with the OCA. However, at larger angles ( $>40$  deg), the effect of increasing the refractive index of cell surroundings on light scattering was much smaller.

Estimations provided by the authors of Ref. 57 allow us to determine the percentage of light scattering from internal cellular structures. Since cells suspended in media with low and high indices have a scattering intensity ratio of 1.3 at angles above 40 deg, it is possible to estimate the fraction of scattering intensity from particles within these cells. In a medium with low refraction, scattering intensity is given by  $I_{nc} + I_c$ , where  $I_{nc}$  and  $I_c$  represent scattering intensities from structures not in contact and in contact with the medium, respectively. In a medium with high refraction, scattering from particles in contact with the medium is reduced by about a factor of 2.1, and scattering is given by  $I_{nc} + 0.48 \cdot I_c$ . Thus, for cells immersed in PBS, relative light scattering from internal cell components is  $I_{nc}/(I_{nc} + I_c) \approx 0.55$ , because  $(I_{nc} + I_c)/(I_{nc} + 0.48 \cdot I_c) \approx 1.3$ .

Note the case of biological cells with well-observable organelles inside. If a corresponding RI ratio exists between these organelles and their environment, they can be trapped.<sup>54,58–60</sup> Optical clearing can provide a better visualization of this trapping process.

A clearing process of the type described in this article enables a more accurate investigation of the inner organelles of complicated living cells.<sup>4</sup> At the same time, knowledge of the scattering properties of single cells allows calculating the bulk properties of solutions or clusters by methods such as Monte-Carlo simulations.<sup>52</sup> However, the fact that the internal structure of RBCs differs from other mammalian cells needs to be considered, when analyzing the effects of optical clearing on light scattering distributions.

The mechanisms of tissue optical clearing by the application of exogenous OCAs still requires more detailed examination.<sup>5–7</sup> Key questions include whether the primary process is a decrease in the scattering coefficient  $\mu_s$  or an increase in the anisotropy  $g$  and whether the change in  $g$  is due to tissue structural changes caused by alteration of particle size or particle packing induced by dehydration.<sup>61,62</sup> In this article, we have directly proved that both the light scattering cross section and the anisotropy factor  $g$  are changed by immersion optical clearing, and that RI matching, as one of the leading optical clearing mechanisms, increases the  $g$  factor. Changes in scatterer size and shape are also important.

## 5 Conclusions

We have shown that optical clearing (RI matching) distinctly affects light scattering distributions around trapped particles. Remarkably, glycerol and glucose increase the RI of the base medium. Another factor that affects scattering distribution is RBC shape variations. Although decreasing the scattering cross section, optical clearing increases optical transmittance and  $g$ .

For medical practice, enhancing light penetration through RBCs by the addition of OCAs could be an exciting new technology for intravascular optical imaging, as proposed and described in Refs. 10, 11, 14, and 32. Effective detection of atherosclerotic plaques using endoscopic OCT with low-molecular weight dextran as clearing agent has already been clinically demonstrated.<sup>33</sup>

## Acknowledgments

The authors wish to express their thanks to TEKES, the Finnish Funding Agency for Technology and Innovation, for financial support via FiDiPro grant 40111/11, to Government of the Russian Federation (grant No. 14.Z50.31.0004 to support scientific research projects implemented under the supervision of

leading scientists) and Russian Presidential grant NSH-703.2014.2. In addition, they would like to thank Dr. A. Popov for his help in sample preparation.

## References

1. R. Barer, K. F. A. Ross, and S. Tkaczyk, "Refractometry of living cells," *Nature* **171**(4356), 720–724 (1953).
2. R. Barer and S. Joseph, "Refractometry of living cells, part 1," *Q. J. Microsc. Sci.* **95**(4), 399–423 (1954).
3. R. Barer and S. Joseph, "Refractometry of living cells, part 2," *Q. J. Microsc. Sci.* **96**(1), 1–26 (1955).
4. C. E. Rommel et al., "Contrast-enhanced digital holographic imaging of cellular structures by manipulating the intracellular refractive index," *J. Biomed. Opt.* **15**(4), 041509 (2010).
5. E. A. Genina, A. N. Bashkatov, and V. V. Tuchin, "Tissue optical immersion clearing," *Expert Rev. Med. Devices* **7**(6), 825–842 (2010).
6. V. V. Tuchin, *Optical Clearing of Tissues and Blood*, p. 256, SPIE, Bellingham, Washington (2006).
7. D. Zhu et al., "Recent progress in tissue optical clearing," *Laser Photonics Rev.* **7**(5), 732–757 (2013).
8. A. Roggan et al., "Optical properties of circulating human blood in the wavelength range 400–2500 nm," *J. Biomed. Opt.* **4**(1), 36–46 (1999).
9. M. C. Meinke, M. Friebel, and J. Helfmann, "Optical Properties of Flowing Blood Cells," Chapter 5 in *Advanced Optical Flow Cytometry*, V. V. Tuchin, Ed., pp. 95–132, Wiley-VCH, Weinheim (2011).
10. V. V. Tuchin, X. Xu, and R. K. Wang, "Dynamic optical coherence tomography in studies of optical clearing, sedimentation, and aggregation of immersed blood," *Appl. Opt.* **41**(1), 258–271 (2002).
11. X. Xu et al., "Effect of dextran-induced changes in refractive index and aggregation on optical properties of whole blood," *Phys. Med. Biol.* **48**(9), 1205–1221 (2003).
12. X. Xu, L. Yu, and Z. Chen, "Effect of erythrocyte aggregation on hematocrit measurement using spectral-domain optical coherence tomography," *IEEE Trans. Biomed. Eng.* **55**(12), 2753–2758 (2008).
13. X. Xu, L. Yu, and Z. Chen, "Optical clearing of flowing blood using dextrans with spectral domain optical coherence tomography," *J. Biomed. Opt.* **13**(2), 021107 (2008).
14. V. V. Tuchin et al., "Theoretical study of immersion clearing of blood in vessels at local hemolysis," *Opt. Express* **12**(13), 2966–2971 (2004).
15. A. N. Bashkatov et al., "Immersion clearing of human blood in the visible and near-infrared spectral ranges," *Opt. Spectrosc.* **98**(4), 638–646 (2005).
16. N. Mohandas et al., "Accurate and independent measurement of volume and hemoglobin concentration of individual red cells by laser light scattering," *Blood* **68**(2), 506–513 (1986).
17. M. Friebel, J. Helfmann, and M. C. Meinke, "Influence of osmolarity on the optical properties of human erythrocytes," *J. Biomed. Opt.* **15**(5), 055005 (2010).
18. H. Ding et al., "Fourier transform light scattering of inhomogeneous and dynamic structures," *Phys. Rev. Lett.* **101**(23), 238102 (2008).
19. Y. Park et al., "Static and dynamic light scattering of healthy and malaria-parasite invaded red blood cells," *J. Biomed. Opt.* **15**(2), 020506 (2010).
20. Y. Kim et al., "Anisotropic light scattering of individual sickle red blood cells," *J. Biomed. Opt.* **17**(4), 040501 (2012).
21. M. T. Valentine et al., "Microscope-based static light scattering instrument," *Opt. Lett.* **26**(12), 890–892 (2001).
22. W. Choi et al., "Field-based angle-resolved light scattering study of single living cells," *Opt. Lett.* **33**(14), 1596–1598 (2008).
23. Y. Park et al., "Refractive index maps and membrane dynamics of human red blood cell parasitized by plasmodium falciparum," *PNAS* **105**(37), 13730–13735 (2008).
24. G. Popescu et al., "Imaging red blood cell dynamics by quantitative phase microscopy," *Blood Cells, Mol. Dis.* **41**(1), 10–16 (2008).
25. G. Popescu et al., "Erythrocyte structure and dynamics quantified by Hilbert phase microscopy," *J. Biomed. Opt.* **10**(6), 060503 (2005).
26. W. H. Wright et al., "Measurement of light scattering from cells using an inverted infrared optical trap," *Proc. SPIE* **1427**, 279–287 (1991).

27. R. M. P. Doornbos et al., "Elastic light scattering measurements of single cells in optical trap," *Appl. Opt.* **35**(4), 729–734 (1996).
28. D. Watson et al., "Elastic light scattering from single cells: orientation dynamics in optical trap," *Biophys. J.* **87**(2), 1298–1306 (2004).
29. M. Collins et al., "Measurement of light scattering from trapped particles," *Proc. SPIE* **7376**, 737619 (2010).
30. M. Kinnunen et al., "Effect of the size and shape of a red blood cell on elastic light scattering properties at the single-cell level," *Biomed. Opt. Express* **2**(7), 1803–1814 (2011).
31. M. Kinnunen et al., "Measurement of elastic light scattering from two optically trapped microspheres and red blood cells in a transparent medium," *Opt. Lett.* **36**(18), 3554–3556 (2011).
32. M. Brezinski et al., "Index matching to improve optical coherence tomography imaging through blood," *Circulation* **103**(15), 1999–2003 (2001).
33. Y. Ozaki et al., "Comparison of contrast media and low-molecular-weight dextran for frequency-domain optical coherence tomography," *Circ. J.* **76**(4), 922–927 (2012).
34. C. F. Bohren and D. R. Huffman, *Absorption and Scattering of Light by Small Particles*, Wiley, New York (1983).
35. R. Graaff et al., "Reduced light scattering properties for mixtures of spherical particles: a simple approximation derived from Mie calculations," *Appl. Opt.* **31**(10), 1370–1376 (1992).
36. A. B. Pravdin et al., "Tissue phantoms," Chapter 5 in *Handbook of Optical Biomedical Diagnostics*, V. V. Tuchin, Ed., pp. 311–352, SPIE Press, Bellingham, Washington (2002).
37. A. Kauppila et al., "Measurement of the trapping efficiency of elliptical optical tweezers with rigid and elastic objects," *Appl. Opt.* **51**(23), 5705–5712 (2012).
38. Philip Laven, "A computer program for scattering of light from a sphere using Mie theory & the Debye series," [www.philiplaven.com](http://www.philiplaven.com) (5 March 2014).
39. A. N. Shvalov et al., "Light-scattering properties of individual erythrocytes," *Appl. Opt.* **38**(1), 230–235 (1999).
40. T. J. Barrett, "Improvement of the indirect hemagglutination assay for salmonella typhi vi antibodies by use of glutaraldehyde-fixed erythrocytes," *J. Clin. Microbiol.* **22**(4), 662–663 (1985).
41. T. Higashi et al., "Orientation of glutaraldehyde-fixed erythrocytes in strong static magnetic fields," *Bioelectromagnetics* **17**(4), 335–338 (1996).
42. S. V. Tsinopoulos and D. Polyzos, "Scattering of He-Ne laser light by an average-sized red blood cell," *Appl. Opt.* **38**(25), 5499–5510 (1999).
43. A. Karlsson et al., "Numerical simulations of light scattering by red blood cells," *IEEE Trans. Biomed. Eng.* **52**(1), 13–18 (2005).
44. M. K. Nilsson et al., "T-matrix computations of light scattering by red blood cells," *Appl. Opt.* **37**(13), 2735–2748 (1998).
45. J. He et al., "Light scattering by multiple red blood cells," *J. Opt. Soc. Am. A* **21**(10), 1953–1961 (2004).
46. N. G. Khlebtsov and S. Yu. Shchegolev, "Allowance for nonspherical particles in determining the parameters of dispersed systems by the turbidity-spectrum method. I. Characteristic scattering functions for systems of nonspherical particles with random orientation in the RDG approximation," *Opt. Spectrosc.* **42**(5), 549–552 (1977).
47. N. G. Khlebtsov and S. Yu. Shchegolev, "Allowance for nonspherical particles in determining the parameters of dispersed systems by the turbidity-spectrum method. II. Characteristic scattering functions for systems of nonspherical particles with random orientation in the van de Hulst approximation," *Opt. Spectrosc.* **42**(6), 663–666 (1977).
48. D. M. Zhestkov et al., "Influence of clearing solutions osmolarity on the optical properties of RBC," *Proc. SPIE* **5474**, 321–330 (2004).
49. A. Kauppila et al., "Elliptical optical tweezers for trapping a red blood cell aggregate," *Photonics Lett. Pol.* **3**(3), 95–97 (2011).
50. A. Ashkin, "Forces of a single-beam gradient laser trap on a dielectric sphere in the ray optics regime," *Biophysical J.* **61**(2), 569–582 (1992).
51. K. O. Greulich, "Micromanipulation by Light in Biology and Medicine," *Methods in Bioengineering*, p. 316, Birkhäuser, Basel, Switzerland (1999).
52. J. Beuthan et al., "The spatial variation of the refractive index in biological cells," *Phys. Med. Biol.* **41**(3), 369–382 (1996).
53. P. Mazon, S. Muller, and H. el Azousi, "Deformation of erythrocytes under shear: a small-angle light scattering study," *Biorheology* **34**(2), 99–110 (1997).
54. A. Ashkin, J. M. Dziedzic, and T. Yamane, "Optical trapping and manipulation of single cell using infrared laser beams," *Nature* **330**(6150), 769–771 (1987).
55. I. Kang-Bin et al., "Optical trapping forces by a focused beam through two media with different refractive indices," *Opt. Commun.* **226**(1–6), 25–31 (2003).
56. H. Felgner, O. Müller, and M. Schliwa, "Calibration of light forces in optical tweezers," *Appl. Opt.* **34**(6), 977–982 (1995).
57. G. C. Salzmann et al., "Light scattering and cytometry," in *Flow Cytometry and Sorting*, 2nd ed., M. R. Melamed, T. Lindmo, and M. L. Mendelsohn, Eds., pp. 81–107, Wiley-Liss Inc., New York (1990).
58. A. Ashkin and J. M. Dziedzic, "Optical trapping and manipulation of viruses and bacteria," *Science* **235**(4795), 1517–1520 (1987).
59. A. Ashkin, "The study of cells by optical trapping and manipulation of living cells using infrared laser beams," *ASGSB Bull.* **4**(2), 133–146 (1991).
60. A. Ashkin and J. M. Dziedzic, "Internal cell manipulation using infrared laser traps (laser cell surgery/optical tweezers/viscoelasticity/mechanical properties/cytoplasmic streaming)," *PNAS* **86**(20), 7914–7918 (1989).
61. R. Samatham, K. G. Phillips, and S. L. Jacques, "Assessment of optical clearing agents using reflectance-mode confocal scanning laser microscopy," *J. Innovative Opt. Health Sci.* **3**(3), 183–188 (2010).
62. S. L. Jacques, R. Samatham, and K. G. Phillips, "Effect of clearing agents on scattering coefficient and anisotropy of scattering of dermis studied by reflectance confocal microscopy," *Proc. SPIE* **7907**, 790706 (2011).

**Matti Kinnunen** received MSc (tech) and DSc (tech) degrees in electrical engineering from the University of Oulu, Oulu, Finland, in 2002 and 2006, respectively. He is currently working as a senior research fellow at the University of Oulu. His research interests include light-matter interactions in tissues and at a single cell level, sensors and measurement techniques as well as optical noninvasive measurement techniques for biomedical applications. He is a board member of Finnish Optical Society.

**Alexander V. Bykov** graduated with honors in 2005 from Moscow State University. He received a PhD degree in 2008 from the same university and a DSc (tech.) degree in 2010 from the University of Oulu, Finland. He is a postdoctoral researcher in the Optoelectronics and Measurement Techniques Laboratory, University of Oulu. His scientific interests are in the area of biophotonics, noninvasive optical diagnostics, theory of light propagation in scattering media, including biotissues and numerical simulation of light transport.

**Juho Tuorila** is currently a MSc (tech) student at the Department of Electrical Engineering, University of Oulu, Finland.

**Tomi Haapalainen** is currently a MSc (tech) student at the Department of Electrical Engineering, University of Oulu, Finland.

**Artashes V. Karmenyan** studied physics and received the University degree in Yerevan State University (YSU), Yerevan, Armenia and the PhD degree in Institute of Radiophysics of Armenian Academy of Science. Later he led the spectroscopy laboratory at R&D Institute "Laserayin Technika" of YSU. In 1994 to 2001, he joined Laboratory of Laser Methods for Diagnosis and Therapy of Tumors, Cancer Research Center, Moscow, Russia. His research interests include laser spectroscopy (Raman, fluorescence, time-resolve), biomedical application, noninvasive optical techniques for research, and reconstruction of early mammalian embryos.

**Valery V. Tuchin** received his MS in radio-physics and electronics (1966), his PhD in optics (1974), and his DSc (1982) in quantum electronics from Saratov State University, Saratov, Russia. Currently, he is a professor and holds the Optics and Biophotonics Chair. He is also a director of the Research-Educational Institute of Optics and Biophotonics at Saratov State University and head of Laboratory on Laser Diagnostics of Technical and Living Systems, Inst. of Precise Mechanics and Control, RAS. His research interests include biophotonics, biomedical optics and laser medicine, physics of optical and laser measurements. In 2007, he was awarded the SPIE Educator Award. He is an SPIE fellow.